Systematic Uncertainties from Gribov Copies in Lattice Calculation of Parton Distributions in the Coulomb Gauge

Xiang Gao[1,2], Jinchen He[3,1*], Rui Zhang[1], and Yong Zhao[1]

[1]*Physics Division, Argonne National Laboratory, Lemont, IL 60439, USA*
[2]*Physics Department, Brookhaven National Laboratory, Upton, NY 11973, USA*
[3]*Maryland Center for Fundamental Physics, University of Maryland, College Park, MD 20742, USA*

(Received 22 August 2024; accepted manuscript online 23 October 2024)

Recently, a new method has been proposed to compute parton distributions using boosted correlators fixed in the Coulomb gauge (CG) within the framework of large-momentum effective theory. This approach, which does not involve Wilson lines, could greatly improve the efficiency and precision of lattice quantum chromodynamics calculations. However, concerns remain regarding whether systematic uncertainties from Gribov copies, which correspond to ambiguities in lattice gauge-fixing, are adequately controlled. This work assesses the effects of Gribov copies on Coulomb-gauge-fixed quark correlators. We utilize different strategies for Coulomb-gauge fixing, selecting two different groups of Gribov copies based on lattice gauge configurations. We examine the differences in the resulting spatial quark correlators in both vacuum and pion states. Our findings indicate that the statistical errors of the matrix elements from both Gribov copies, regardless of the correlation range, decrease proportionally to the square root of the number of gauge configurations. The difference between the strategies does not show statistical significance compared to the gauge noise, demonstrating that the effect of the Gribov copies can be neglected in practical lattice calculations of quark parton distributions.

DOI: 10.1088/0256-307X/41/12/121201

1. Motivation. Understanding the 3D partonic structure of the proton is a primary goal of experiments at RHIC,[1] Jefferson Lab,[2] Fermilab,[3,4] CERN[5] and the future electron-ion collider.[6,7] In recent years, significant progress has been made toward 3D tomography of hadrons using lattice quantum chromodynamics (QCD).[8] Among various approaches, large-momentum effective theory (LaMET)[9–11] provides a first-principle framework to calculate the x-dependence of all parton distributions, leading to substantial lattice results on parton distribution functions (PDFs), generalized parton distributions (GPDs), and transverse-momentum-dependent distributions (TMDs) (see, for example, Refs. [12–17]).

In the LaMET framework, the light-cone parton distribution is approached through a quasi-distribution defined by an equal-time correlator of quarks or gluons in a boosted hadron state, typically contracted with a Wilson line that makes it gauge invariant. In the TMD case, the Wilson line consists of two longitudinal gauge links with a long extension and a transverse link that closes the contour to ensure gauge invariance. For long-range correlations, the self-energy of the Wilson lines causes an exponential suppression of the signal-to-noise ratio in lattice simulations owing to linear power divergences,[18–20] limiting computational precision, especially for TMDs in the nonperturbative region.

Recently, a new method was proposed to compute parton distributions from correlators fixed in the Coulomb gauge (CG) without using Wilson lines.[21–23] These boosted CG correlators belong to the same universality class[11,24] as gauge-invariant quasi-distributions and can, therefore, be matched to light-cone TMDs through LaMET.[22,25–28] The CG method can significantly alleviate the suppression of the signal-to-noise ratio in long-range correlations, thus dramatically improving the precision of TMD calculations. Moreover, the lattice renormalization of the correlators is substantially simplified with the absence of linear divergence and the reduction of operator mixings.[21] The 3D rotational symmetry of the CG condition allows access to the same hadron momentum from an off-axis direction with less computational cost.[21] Nevertheless, there are concerns regarding whether the CG fixing process introduces additional uncontrollable systematic uncertainties. The main uncertainty comes from the effect of Gribov copies,[29,30] which are multiple solutions on a gauge orbit that satisfy the CG condition. Since the standard lattice gauge-fixing algorithm[31,32] does not uniquely fix the CG, it is important to determine if the variation in gauge-dependent matrix elements due to different Gribov copies is significant. If this variation is much smaller than the statistical errors from averaging over the set of gauge configurations in lattice simulations, then Gribov copies do not pose a practical problem for their application in parton physics. This work aims to assess the systematic uncertainty from Gribov copies for CG quark correlators.

In lattice QCD calculations, the path integral in the continuum theory is replaced by an ordinary integral over the gauge link variables $U_\mu(x)$ on a finite lattice. This allows gauge-invariant quantities to be calculated nonper-

*Corresponding author. Email: jinchen@umd.edu
© 2024 Chinese Physical Society and IOP Publishing Ltd

turbatively without the need for gauge fixing. Gauge fixing is only required when calculating gauge-dependent quantities, such as quark propagators. To fix the gauge on the lattice, the standard method involves finding the extreme point of a specific functional.[31,32] For example, we consider the CG. In continuum theory, one can define a functional as follows:

$$F_{\rm CG}[A,\,\Omega] \equiv \frac{1}{2}\sum_{\mu=1}^{3}\int d^4x A^a_{\Omega\mu}(x)A^{\mu a}_{\Omega}(x), \tag{1}$$

where a is the SU(3) color index in the adjoint representation, $A_{\Omega\mu}(x) \equiv \Omega^\dagger(x)A_\mu(x)\Omega(x) + \frac{i}{g}\Omega^\dagger(x)\partial_\mu\Omega(x)$, and $\Omega(x)$ denotes a gauge transformation. If an infinitesimal gauge transformation θ is applied to the gauge potential $A_{\Omega\mu}$,

$$\delta A_{\Omega\mu} = -D^{\Omega}_{\mu ab}\theta_b = -(\partial_\mu\theta_a - g f^{cab}A^c_{\Omega\mu}\theta_b), \tag{2}$$

then the variation of the functional is as follows:

$$\begin{aligned}\delta F_{\rm CG}[A,\,\Omega] &= -\sum_{\mu=1}^{3}\int d^4x(\partial_\mu\theta_a - g f^{cab}A^c_{\Omega\mu}\theta_b)A^{\mu a}_{\Omega}\\ &= \sum_{\mu=1}^{3}\int d^4x\theta_a(\partial_\mu A^{\mu a}_{\Omega}).\end{aligned} \tag{3}$$

Therefore, if the functional reaches an extreme point, the CG condition $\sum_{\mu=1}^{3}\partial_\mu A^{\mu a}_{\Omega} = 0$ is satisfied. On the lattice, the discretized version of the functional is[31]

$$F[U,\,\Omega] \equiv -{\rm Re}\Big[{\rm Tr}\sum_x\sum_{\mu=1}^{l}\Omega^\dagger(x+\hat{\mu})U_\mu(x)\Omega(x)\Big], \tag{4}$$

where $l = 4$ for the Landau gauge and $l = 3$ for the CG.

However, as shown by Gribov[29] and Singer,[30] the extrema of the functional are not unique, leading to what are known as Gribov copies. The impact of Gribov copies on lattice calculations generally falls into two categories: measurement distortion and lattice Gribov noise, with the latter being inseparable from the statistical uncertainty of the Monte Carlo simulations. An illustrative example of a distortion caused by Gribov copies can be observed in the evaluation of the photon propagator in compact U(1) within the Coulomb phase.[33] The impact of Gribov copies has been widely discussed in the literature,[34–38] showing that the gluon propagator in the far infrared region is influenced by Gribov copies in SU(2) gauge theory.[36,39] Interestingly, in the quark propagator sector, Gribov noise was found to be negligible compared to statistical noise.[40,41]

The paper is organized as follows. Our methodology for generating different Gribov copies and assessing their systematic uncertainties is detailed in Section 2. The numerical results for the pion valence quark quasi-distributions and the light-quark spatial propagator are presented in Section 3. Finally, in Section 4, we conclude that the systematic uncertainties from Gribov copies are negligible compared to the statistical noise from averaging over gauge configurations, thus solidifying the CG correlator approach for calculating parton physics.

2. Methodology. Various techniques for generating different Gribov copies have been discussed in the literature.[35] One such method, known as the mother-and-daughter approach, involves applying n distinct random gauge transformations to a mother configuration M, followed by fixing these transformed configurations to a particular gauge to produce n daughter configurations $\{M_1, M_2, \ldots, M_n\}$. These daughters can potentially access up to n distinct Gribov copies, although multiple daughters may correspond to the same Gribov copy. An alternative approach involves using the overrelaxation algorithm,[42] where different choices of the overrelaxation parameter can lead to different Gribov copies, even starting from the same initial configuration.[35] In this work, we adopt the mother-and-daughter method to generate different Gribov copies for each initial configuration. This method has also been used in high-precision lattice calculations of nucleon axial coupling.[43]

As mentioned in Section 1, different Gribov copies correspond to different extrema of the functional, representing different gauge transformations. A straightforward way to distinguish these copies is by comparing the gauge transformations used for gauge fixing. However, directly comparing two high-dimensional vectors is impractical. Instead, we can define a one-dimensional quantity to serve as a useful criterion. A good criterion is the functional value F after gauge fixing. Variations beyond the accuracy of gauge fixing indicate a distinct extremum, representing a new Gribov copy. There are two possible criteria for the precision of gauge fixing: one is the normalized variation in the functional $\delta F/F$; the other is the residual gradient of the functional defined as[35]

$$\theta^G \equiv \frac{1}{V}\sum_x\theta^G(x) \equiv \frac{1}{V}\sum_x{\rm Tr}[\Delta^G(x)(\Delta^G)^\dagger(x)], \tag{5}$$

where V is the lattice volume, and the gradient is defined as $\Delta^G(x) \equiv \sum_\mu(A^G_\mu(x) - A^G_\mu(x-\hat{\mu}))$. Both criteria approach zero under the gauge-fixing condition. In this work, we adopt the first criterion, allowing us to distinguish different copies according to the value of F after gauge fixing.

The numerical effects introduced by Gribov copies can be categorized into two primary types: lattice Gribov noise and measurement distortion.[35] Lattice Gribov noise arises from residual gauge freedoms and relates to the distribution of lattice measurements all Gribov copies. This noise is indistinguishable from the statistical uncertainties that arise from variations among lattice configurations.[44,45] Consequently, the predominant concern regarding Gribov copies is the resultant measurement distortion. This distortion is linked to the choice of the representative within various Gribov copies during gauge fixing, i.e., the gauge-fixing strategy. A biased strategy can result in deviations from the true value, even though Gribov noise remains indistinguishable from statistical uncertainties. For example, selecting the copy with the maximal lattice measurement value as the representative for each configuration will clearly produce a distorted measurement. Therefore, it is necessary to quantify measurement distortion, and a standard approach in the literature is to employ various gauge-fixing strategies for comparative analysis. The resultant discrepancies among these strategies provide an estimation of the measurement distortion. As an illustration, Ref. [36] examines two distinct

strategies for gauge fixing: Absolute gauge fixing involves identifying the absolute minimum of the functional, approximated using the algorithm detailed in App. B of the reference; Minimal gauge fixing selects an arbitrary copy in the first Gribov region, where the Faddeev–Popov operator is positive definite.[46] This minimal gauge-fixing strategy is the most popular choice in lattice calculations. Ref. [39] evaluates three additional strategies: simulated annealing (SA), best copy; SA, first copy; and flipped simulated annealing (FSA), best copy. SA is an algorithm that improves the efficiency of standard overrelaxation. The term "flipped" refers to applying a $\mathbb{Z}(2)$ flip transformation[39] on the gauge configuration. Without "flipped", all copies are constrained in the first Gribov region. "best copy" means choosing the copy with the maximum functional value among all obtained copies, while "first copy" refers to the first copy fixed by the FSA or SA algorithm.

Further investigation into strategies for selecting the Gribov copies during gauge fixing can be found in Ref. [47–51]. Among these approaches, the flip transformations $\mathbb{Z}(2)$, first introduced in the context of Landau gauge fixing in Ref. [52], differ from conventional gauge fixing methods. However, in lattice calculations of hadron structure functions, flip transformations are rarely used, so the $\mathbb{Z}(2)$ flip is not studied in this work.

Considering the computational cost of $3+1$ dimensional QCD simulations on the lattice, we study two strategies in this work:

1. First instance ("First it"): choosing the first copy obtained in the first Gribov region;
2. Smallest functional ("Smallest f"): choosing the copy with the smallest functional value among all obtained copies in the first Gribov region.

By applying these two strategies, we should obtain two different sets of configurations after fixing the CG. The measurement distortion introduced by the Gribov copies is estimated by comparing these two sets.

Table 1. Comprehensive overview of the lattice configuration and measurement parameters. Symbol #Cfgs denotes the number of configurations, while #It represents the frequency of gauge-fixing instances per configuration. Furthermore, #ex and #sl indicate the counts of the precise inversions and the approximate inversions, respectively. We have specified the bare Wilson fermion quark mass $m_q a$ corresponding to a 300 MeV pion mass m_π, the temporal extent L_t of the lattice in m_π units.

a	$L_s^3 \times L_t$	$m_q a$	$m_\pi L_t$	#Cfgs	#It	(#ex, #sl)
0.06 fm	$48^3 \times 64$	−0.0388	5.85	100	8	(1, 8)

3. Numerical results. To estimate the impact of Gribov copies, we performed a numerical lattice QCD calculation on a $2+1$ flavor QCD gauge ensemble generated by the HotQCD Collaboration[53] using highly improved staggered quarks (HISQ).[54] The ensemble features a lattice spacing of $a = 0.06$ fm and a volume of $L_s^3 \times L_t = 48^3 \times 64$. We used tadpole-improved clover Wilson valence fermions on a hypercubic (HYP) smeared[55] gauge background. We set the clover coefficient $c_{\rm sw} = u_0^{-3/4}$, where u_0 is the average plaquette after HYP smearing. The parameter is set as $c_{\rm sw} = 1.0336$ for both time and spatial directions. For the valence quark masses, we used $\kappa \approx 0.12623$ for the light quarks u and d, corresponding to a valence pion mass $m_\pi = 300$ MeV. We measured 100 gauge configurations and effectively increased the statistics eightfold by using one exact Dirac operator inversion (with precision 10^{-10}) and eight sloppy inversions (with precision 10^{-4}) on each configuration using all-mode averaging (AMA).[56] The details of the measurements are collected in Table 1. Using this set-up, the statistical uncertainties associated with the matrix elements are maintained at subpercent level, which is sufficient for examining the systematic uncertainties from the Gribov copies. Using the mother-and-daughter methodology referenced in Section 2, we employ the steepest descent algorithm to obtain eight instances of functional minima for each configuration. In the case of the minimal functional F, the determinant of the Faddeev–Popov operator is non-negative, ensuring all instances are in the first Gribov region.[35] A recent paper[57] shows that gauge-dependent measurements are highly sensitive to gauge-fixing precision. Only with high precision can the continuum limit be observed among the results from different lattice ensembles, as demonstrated in our previous work in Ref. [21]. Therefore, in this work, we choose a high precision of $\delta F/F \leq 10^{-8}$ for gauge fixing in each configuration. Different copies are distinguished by functional values that exceed the precision of the gauge fixing. Two sets of Gribov copies are selected on 100 configurations according to the strategies mentioned in Section 2, named "First it" and "Smallest f", respectively.

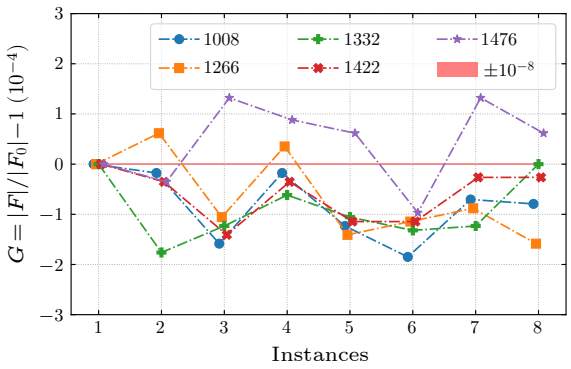

Fig. 1. Distribution of functional values across five configurations, with the x-axis showing eight instances of gauge fixing.

As illustrated in Fig. 1, five configurations (configuration numbers: 1008, 1266, 1332, 1422, and 1476) were randomly selected. Relative differences in the absolute functional values, defined as $G = |F|/|F_0| - 1$, are plotted for each gauge-fixing instance. Here, $|F|$ represents the absolute functional values of each instance, and $|F_0|$ is the absolute functional value of instance 1008. Given that the precision of the gauge fixing is set to $\delta F/F \leq 10^{-8}$, instances where the relative difference G exceeds 10^{-8} are identified as distinct Gribov copies. As shown in Fig. 1, the red band represents the range of 10^{-8}, clearly indicating that most instances belong to distinct copies. Consequently, the methodology used for selecting various Gribov copies is demonstrated to be effective in these configura-

tions.

3.1. Quark Propagator. Most lattice QCD calculations start from measuring correlations. To assess the impact of Gribov copies, we measured light-quark propagators at different separations z using a point source and a point sink in the coordinate space. Since the gauge is independently fixed on each time slice, light-quark propagators are chosen along a spatial direction to ensure a nonvanishing signal. The light-quark propagator is defined as follows:

$$C_u(z) = \langle \mathrm{Tr}[u(z)\bar{u}(0)] \rangle, \tag{6}$$

where Tr denotes the trace over both the color and spin indices. The decaying behavior of $C_u(z)$ can be presented more clearly by defining the effective mass m_{eff} of the dressed quark at each z as[58] through

$$\frac{C_u(z)}{C_u(z+1)} = \frac{\cosh(m_{\mathrm{eff}} \cdot (z - L_s/2))}{\cosh(m_{\mathrm{eff}} \cdot (z + 1 - L_s/2))}, \tag{7}$$

where L_s is the lattice size in the spatial directions. Both the two-point correlation functions and the effective masses of the two gauge-fixing strategies are shown in Fig. 2, with uncertainties estimated using bootstrap resampling 100 bootstrap samples are included in this work. The plots demonstrate good consistency between the two sets, indicating that the measurement distortions from the Gribov copies are smaller than the statistical noise.

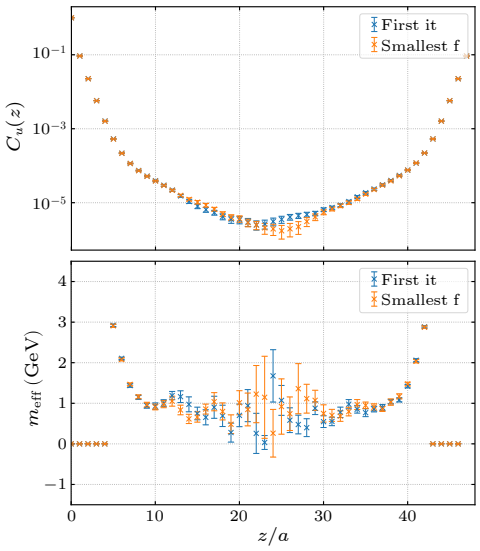

Fig. 2. Two-point correlation functions(up) and the effective mass of the quark spatial propagator(down) using two different strategies are plotted. The uncertainties are estimated using bootstrap resampling on 100 configurations.

Considering that imprecise gauge fixing or a skewed gauge-fixing strategy could result in a complex and irregular distribution of lattice measurements across different configurations and Gribov copies, error estimation with a finite number of configurations requires careful evaluation. To verify that our number of configurations is sufficient for accurate error estimation, the errors of $C_u(z)$ and $m_{\mathrm{eff}}(z = 10a)$ are plotted as functions of the number of configurations N in Fig. 3. It is well known that statistical uncertainties decrease according to $1/\sqrt{N}$ as the number of configurations N increases. Observing a consistent pattern suggests that our bootstrap samples are sufficient to describe the distribution of the quark spatial propagator across different configurations and Gribov copies, and increasing the number of measurements can achieve higher precision. Moreover, this serves as supporting evidence that our gauge-fixing precision is sufficiently high. The gray bands in the figures show the expected error as $C_u(N = 10)/\sqrt{N}$ and $m_{\mathrm{eff}}(N = 10)/\sqrt{N}$, respectively. The data from both "First it" and "Smallest f" align well with the expected error, indicating that the errors generally behave as statistical noise with negligible systematic uncertainties from the Gribov copies.

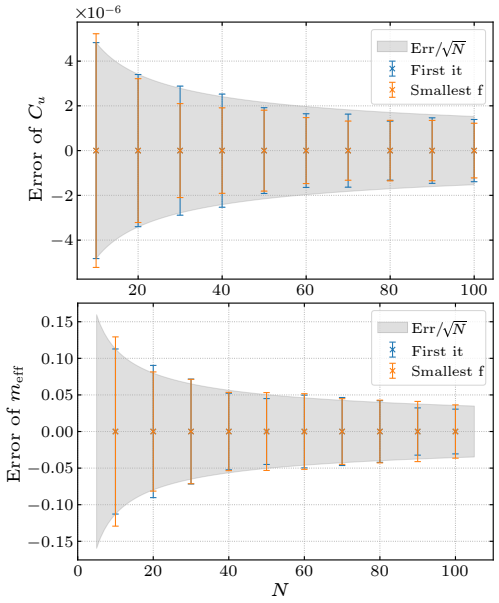

Fig. 3. Errors of the quark propagator and the effective mass at $z = 10a$ as a function of the number of configurations N. The gray band shows the expected error that decreases as $1/\sqrt{N}$.

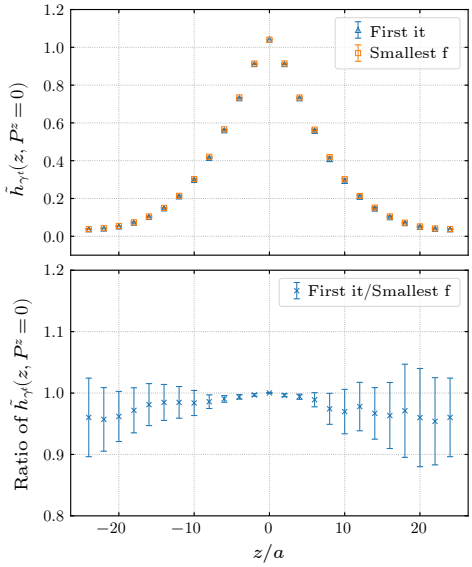

Fig. 4. Upper panel: z-dependence of the pion quasidistribution matrix element using each strategy. Lower panel: z-dependence of the ratio of matrix elements using the two strategies.

3.2. Quasi-Distribution Matrix Elements. To further investigate the systematic uncertainties of Gribov copies, specifically in the lattice calculation of parton physics, we calculate the spatial correlators for pion quasidistributions using the two groups of Gribov copies mentioned above. Owing to the 3D rotational invariance under the CG, the correlators can be used to define both PDFs[21] and TMDs.[22,23]

The bare quasidistribution matrix element under the CG is[21]

$$\tilde{h}_{\gamma^t}(z, P^z, \mu) = \frac{1}{2P^t}\langle P|\bar{\psi}(z)\gamma^t\psi(0)|_{\boldsymbol{\nabla}\cdot\boldsymbol{A}=0}|P\rangle, \quad (8)$$

which can be extracted from the ratio of the three-point correlations and the two-point correlations (see App. A). Without loss of generality, we focus on the $P^z = 0$ matrix elements of the pion, which are the least computationally expensive. Three time separations, $t_{\rm sep} = \{8, 10, 12\}a$, are measured for the three-point correlations $C_{\rm 3pt}(t_{\rm sep})$. To eliminate excited-state contamination, we fit the two-point correlations $C_{\rm 2pt}(t)$ with two energy states in $t \in [3, 15]$. Then, the fit posteriors are then used as priors in the two-state fit of the ratio $R(t_{\rm sep}, \tau) = C_{\rm 3pt}(t_{\rm sep}, \tau)/C_{\rm 2pt}(t_{\rm sep})$, where τ is the insertion time of the operator. All fits are least-square fits based on Bayesian analysis. Bootstrap resampling, with 100 samples, is adopted to establish correlations among all data points, maintaining consistency throughout the analysis, similarly to the quark propagator analysis.

To compare the calculations using the two different strategies, we plot the bare matrix elements and their ratios in Fig. 4, which demonstrate good consistency within 1σ. To illustrate the statistical comparison between the two sets in detail, we select four typical separations

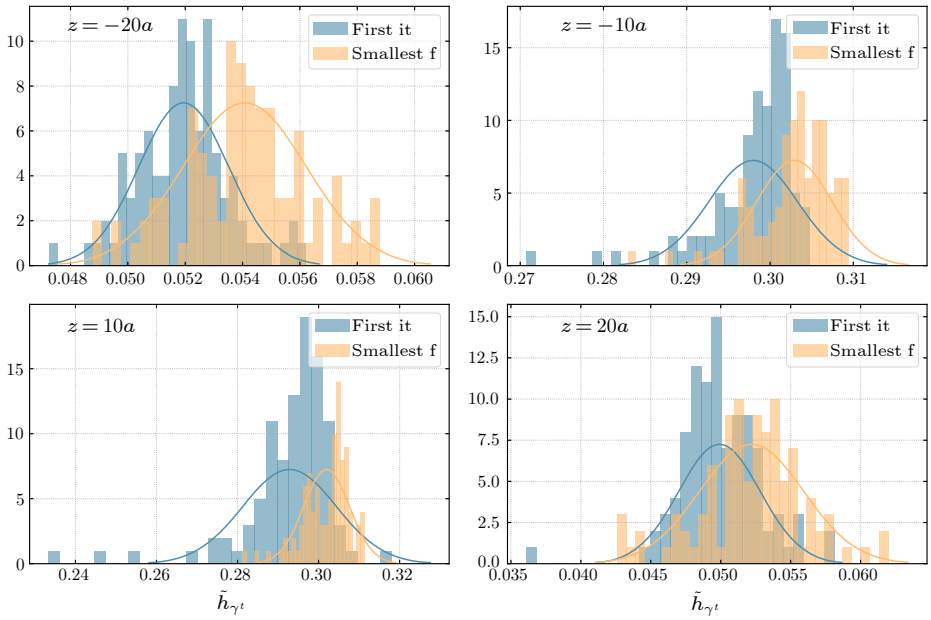

Fig. 5. Histograms of matrix element $\tilde{h}_{\gamma^t}(z, P^z = 0)$ from bootstrap samples of 100 configurations, measured on two different sets of Gribov copies.

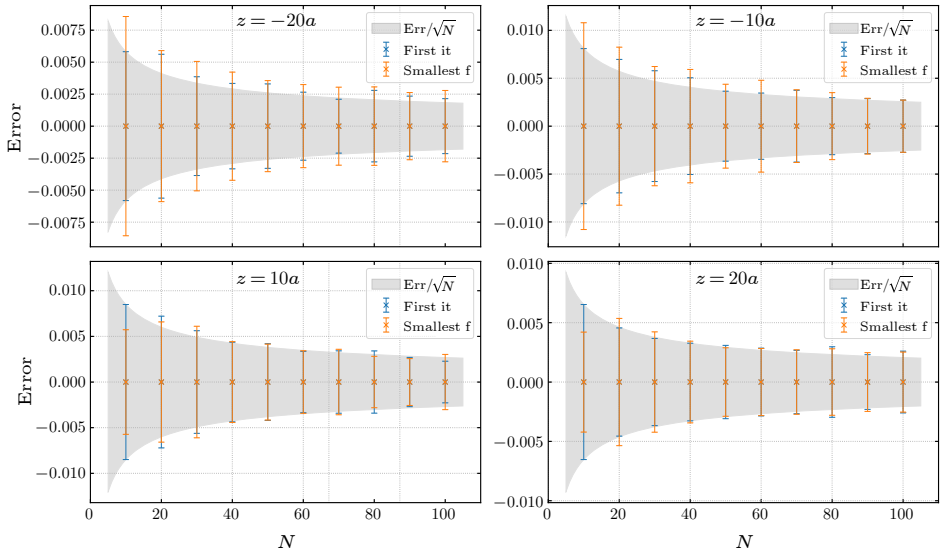

Fig. 6. Error of the ratio at different separations z, $t_{\rm sep} = 8a$ and $\tau = 4a$. Varying N corresponds to using different numbers of configurations, each resampled via bootstrap to obtain 100 samples.

$z = \{-20, -10, 10, 20\}a$ and plot histograms from bootstrap samples of the matrix elements in Fig. 5. The matrix elements show no statistical difference between the two strategies for choosing Gribov copies in the gauge-fixing process, suggesting that the measurement distortion of the Gribov copies is smaller than the statistical uncertainties.

Similarly to Fig. 3, we assess our error estimation by examining how uncertainties vary with the number of configurations. We plot the error of the ratio $R(t_{\text{sep}} = 8a, \tau = 4a)$ for various separations z in Fig. 6. The gray band represents the expected error as $R(N = 10)/\sqrt{N}$, which aligns with both sets of Gribov copies. This shows that the error estimation for both the "First iteration" and the "Smallest functional", as defined in Section 2, is reliable.

4. Conclusion. In conclusion, this work assessed the effect of Gribov copies on the measurements of quark correlators in CG by comparing two different strategies: "First it" and "Smallest f") in gauge fixing. Our results on the quark propagator and the quasi-distribution matrix elements show that the systematic uncertainties from Gribov copies, i.e., measurement distortions, are negligible compared with the statistical uncertainties in the CG matrix elements. This finding is consistent with the argument in Ref. [21] and supports the effectiveness of the CG method in calculating parton physics. It should be noted that the results in this work are under a finite precision of gauge fixing. According to Ref. [57], although the precision $\delta F/F \leq 10^{-8}$ is sufficient for CG quark correlations, the imperfect gauge fixing may also contribute to the minor measurement distortion in our results, which can be reduced by improving the precision.

In the future, more instances of gauge fixing, i.e., more Gribov copies, can be included to examine the full extent of the measurement distortion. The recent study in Ref. [41] deployed 100 copies to analyze the influence of Gribov copies on the quark propagator, although being limited to two colors. Furthermore, other strategies can be explored to select diverse Gribov copies to strengthen our conclusions. Moreover, the effect of Gribov copies on CG gluon correlators, which has been studied for gluon propagators in SU(2) gauge theory,[36,39] will be investigated in SU(3) QCD for their application in gluon parton distributions.

Acknowledgements. Correlator measurements were carried out with the `Qlua` software suite,[59] which utilized the multigrid solver in `QUDA`.[60,61] Some calculations were performed using the `Grid`[62,63] and `GPT` [64] software packages.

We thank George Flemming, Xiangdong Ji, Peter Petreczky, Swagato Mukherjee, and Dennis Bollweg for their valuable communications. This material is based on work supported by the U.S. Department of Energy, Office of Science, Office of Nuclear Physics through Contract Nos. DE-AC02-06CH11357 and DE-SC0012704, and within the frameworks of Scientific Discovery through Advanced Computing (SciDAC) award *Fundamental Nuclear Physics at the Exascale and Beyond* and the Quark-Gluon Tomography (QGT) Topical Collaboration, under contract No. DE-SC0023646. YZ is also partially supported by the 2023 Physical Sciences and Engineering (PSE) Early Investigator Named Award program at Argonne National Laboratory.

This research used awards of computer time provided by the INCITE program at the Argonne Leadership Computing Facility, a DOE Office of Science User Facility operated under Contract DE-AC02-06CH11357, the ALCC program at the Oak Ridge Leadership Computing Facility, which is a DOE Office of Science User Facility supported under Contract DE-AC05-00OR22725, the National Energy Research Scientific Computing Center, a DOE Office of Science User Facility supported by the Office of Science of the U.S. Department of Energy under Contract DE-AC02-05CH11231 using NERSC award NP-ERCAP0028137. Computations for this work were carried out in part on the facilities of the USQCD Collaboration, which is funded by the Office of Science of the U.S. Department of Energy. We gratefully acknowledge the computing resources provided on Swing, a high-performance computing cluster operated by the Laboratory Computing Resource Center at Argonne National Laboratory.

References

[1] Aschenauer E C, Barish K, Bazilevsky A *et al.* 2023 arXiv:2302.00605 [nucl-ex]
[2] Dudek J, Ent R, Essig R *et al.* 2012 *Eur. Phys. J. A* **48** 187
[3] Aidala C A, Arrington J R, Ayuso C *et al.* 2019 *Nucl. Instrum. Methods Phys. Res. Sect. A* **930** 49
[4] Chen A, Peng J C, Leung C H *et al.* 2019 *Proc. Sci.* **346** 164
[5] Abbon P, Albrecht E, Alexakhin V Y *et al.* 2007 *Nucl. Instrum. Methods Phys. Res. Sect. A* **577** 455
[6] Accardi A, Albacete J L, Anselmino M *et al.* 2016 *Eur. Phys. J. A* **52** 268
[7] Abdul Khalek R, Accardi A, Adam J *et al.* 2022 *Nucl. Phys. A* **1026** 122447
[8] Constantinou M, Courtoy A, Ebert M A *et al.* 2021 *Prog. Part. Nucl. Phys.* **121** 103908
[9] Ji X D 2013 *Phys. Rev. Lett.* **110** 262002
[10] Ji X D 2014 *Sci. China Phys. Mech. Astron.* **57** 1407
[11] Ji X D, Liu Y Z, Liu Y S, Zhang J H, and Zhao Y 2021 *Rev. Mod. Phys.* **93** 035005
[12] Gao X, Hanlon A D, Mukherjee S, Petreczky P, Scior P, Syritsyn S, and Zhao Y 2022 *Phys. Rev. Lett.* **128** 142003
[13] Yao F, Walter L, Chen J W *et al.* 2023 *Phys. Rev. Lett.* **131** 261901
[14] Bhattacharya S, Cichy K, Constantinou M, Dodson J, Gao X, Metz A, Mukherjee S, Scapellato A, Steffens F, and Zhao Y 2022 *Phys. Rev. D* **106** 114512
[15] Holligan J and Lin H W 2023 arXiv:2312.10829 [hep-lat]
[16] He J C, Chu M H, Hua J, Ji X, Schäfer A, Su Y, Wang W, Yang Y B, Zhang J H, and Zhang Q A 2024 *Phys. Rev. D* **109** 114513
[17] Avkhadiev A, Shanahan P E, Wagman M L, and Zhao Y 2024 *Phys. Rev. Lett.* **132** 231901
[18] Ji X, Zhang J H, and Zhao Y 2018 *Phys. Rev. Lett.* **120** 112001
[19] Ishikawa T, Ma Y Q, Qiu J W, and Yoshida S 2017 *Phys. Rev. D* **96** 094019
[20] Green J, Jansen K, and Steffens F 2018 *Phys. Rev. Lett.* **121** 022004
[21] Gao X, Liu W Y, and Zhao Y 2023 arXiv:2306.14960 [hep-ph]
[22] Zhao Y 2023 arXiv:2311.01391 [hep-ph]
[23] Bollweg D, Gao X, Mukherjee S, and Zhao Y 2024 *Phys. Lett. B* **852** 138617
[24] Hatta Y, Ji X, and Zhao Y 2014 *Phys. Rev. D* **89** 085030

[25] Ebert M A, Stewart I W, and Zhao Y 2019 *J. High Energ. Phys.* **2019** 37
[26] Ji X, Liu Y, and Liu Y S 2020 *Nucl. Phys. B* **955** 115054
[27] Ji X, Liu Y, and Liu Y S 2020 *Phys. Lett. B* **811** 135946
[28] Ebert M A, Schindler S T, Stewart I W, and Zhao Y 2022 *J. High Energ. Phys.* **2022** 178
[29] Gribov V N 1978 *Nucl. Phys. B* **139** 1
[30] Singer I M 1978 *Commun. Math. Phys.* **60** 7
[31] Mandula J E and Ogilvie M 1987 *Phys. Lett. B* **185** 127
[32] Davies C T H, Batrouni G G, Katz G R, Kronfeld A S, Lepage G P, Wilson K G, Rossi P, and Svetitsky B 1988 *Phys. Rev. D* **37** 1581
[33] Petrarca S 2000 arXiv:hep-lat/9912037
[34] Bali G S, Bornyakov V, Müller-Preussker M, and Schilling K 1996 *Phys. Rev. D* **54** 2863
[35] Giusti L, Paciello M L, Petrarca S, Taglienti B, and Parrinello C 2001 *Int. J. Mod. Phys. A* **16** 3487
[36] Maas A 2009 *Phys. Rev. D* **79** 014505
[37] Burgio G, Quandt M, Reinhardt H, and Vogt H 2017 *Phys. Rev. D* **95** 014503
[38] Golterman M, Greensite J, Peris S, and Szczepaniak A P 2012 *Phys. Rev. D* **85** 085016
[39] Bornyakov V G, Mitrjushkin V K, and Rogalyov R N 2012 *Phys. Rev. D* **86** 114503
[40] Burgio G, Schröck M, Reinhardt H, and Quandt M 2012 *Phys. Rev. D* **86** 014506
[41] Kalusche G, Lawlor D, and Skullerud J I 2024 arXiv:2405.17301[hep-lat]
[42] Mandula J E and Ogilvie M 1990 *Phys. Lett. B* **248** 156
[43] Chang C C *et al.* 2018 *Nature* **558** 91
[44] Martinelli G, Petrarca S, Sachrajda C T, and Vladikas A 1993 *Phys. Lett. B* **311** 241 [Erratum: 1993 *Phys. Lett. B* **317** 660]
[45] Paciello M L, Petrarca S, Taglienti B, and Vladikas A 1994 *Phys. Lett. B* **341** 187
[46] Vandersickel N and Zwanziger D 2012 *Phys. Rept.* **520** 175
[47] Parrinello C and Jona-Lasinio G 1990 *Phys. Lett. B* **251** 175
[48] Zwanziger D 1990 *Nucl. Phys. B* **345** 461
[49] Bogolubsky I L, Bornyakov V G, Burgio G, Ilgenfritz E M, Müller-Preussker M, and Mitrjushkin V K 2008 *Phys. Rev. D* **77** 014504 [Erratum: 2008 *Phys. Rev. D* **77** 039902]
[50] Bogolubsky I L, Ilgenfritz E M, Müller-Preussker M, and Sternbeck A 2009 *Phys. Lett. B* **676** 69
[51] Bornyakov V G and Mitrjushkin V K 2012 *Int. J. Mod. Phys. A* **27** 1250050
[52] Bogolubsky I L, Burgio G, Müller-Preussker M, and Mitrjushkin V K 2006 *Phys. Rev. D* **74** 034503
[53] Bazavov A, Bhattacharya T, DeTar C *et al.* 2014 *Phys. Rev. D* **90** 094503
[54] Follana E, Mason Q, Davies C, Hornbostel K, Lepage G P, Shigemitsu J, Trottier H, and Wong K 2007 *Phys. Rev. D* **75** 054502
[55] Hasenfratz A and Knechtli F 2001 *Phys. Rev. D* **64** 034504
[56] Shintani E, Arthur R, Blum T, Izubuchi T, Jung C, and Lehner C 2015 *Phys. Rev. D* **91** 114511
[57] Zhang K, Huo Y K, Ji X D, Schaefer A, Shi C J, Sun P, Wang W, Yang Y B, and Zhang J H 2024 arXiv:2405.14097 [hep-lat]
[58] Gattringer C and Lang C B 2010 *Quantum chromodynamics on the lattice* **788** (Springer Berlin)
[59] Pochinsky A 2008 Qlua lattice software suite (2008-present)
[60] Clark M A, Babich R, Barros K, Brower R C, and Rebbi C 2010 *Comput. Phys. Commun.* **181** 1517
[61] Babich R, Clark M A, Joó B, Shi G, Brower R C, and Gottlieb S 2011 arXiv:1109.2935 [hep-lat]
[62] Boyle P A, Cossu G, Yamaguchi A, and Portelli A 2016 *Proc. Sci.* **251** 023
[63] Yamaguchi A, Boyle P, Cossu G, Filaci G, Lehner C, and Portelli A 2022 *Proc. Sci.* **396** 035
[64] Lehner C *et al.* Grid python toolkit (gpt)